MMP Modeling Techniques with Curved Line Multipoles

P. Leuchtmann
ETH Zurich, CH-8092 Zurich, Switzerland

Abstract: *The MMP modeling of different scattering structures is discussed. It is shown that highly accurate near and farfield simulations are possible, not only for simple academic structures such as spheres or cubes, but also for a multiturn helical wire of finite thickness and an absorbing ferrite cylinder placed on a cable. Some typical problem classifying figures (symmetry, error, number of equations, matching points etc.) are defined in order to classify and compare different problems. MMP's symmetry exploitation concept (reducing both memory and cpu time) is explained. Although the amount of calculation increases when edges or tips are present, rather small radii of curvature may be treated using (curved or straight) line multipoles.*

1 Introduction

The MMP program package [1,2,3] (multiple multipole program) is a frequency domain tool for computational electromagnetics with piecewise homogeneous, linear and isotropic, possibly lossy materials. The basic MMP-approach consists of a series expansion of the unknown electromagnetic field using (two-vector-valued) expansion functions which are solutions of Maxwell's homogeneous equations. 'Homogeneous' has two meanings here: 1. 'no impressed sources', i.e., no impressed charge density ϱ and no impressed current density $\vec{j}$ and 2. no spacial (and time) variation of the material parameters. Since material properties may change from subdomain to subdomain, all expansion functions are restricted to a single subdomain. Impressed sources may be taken into account by including their fields in the 'zero-th term' of the expansion (excitation).

An intelligent choice of the expansion functions keeps their number low and therefore yields a low number of unknowns. Since the original multipole expansions (we call them point multipoles or conventional multipoles) are excellent for sphere-like structures, but less efficient for thin wires, edges and corners, special expansion functions ('line multipoles') have been developed for the latter cases [3,4]. The purpose of this paper is

- to give a short description on the behavior of both point and line multipole functions,
- to show how the MMP modeling process is modified when line multipoles are used, possibly beside conventional multipoles and other expansion functions,
- to discuss the advantages and drawbacks of the line multipoles vs. the point multipoles in different applications,
- to discuss the solutions for the solved problems.

Starting with MMP's most simple example (scattering at a sphere), we shall describe the modeling of more complicated structures and show the increase of both memory requirements and computation time when the structure deviates from a sphere and when dielectric, lossy or magnetic materials are involved.

The use of geometrical *symmetries* — even if the field itself is not symmetrical — reduces both memory requirements and computation time. MMP decomposes the full problem in up to eight (even and/or odd) symmetrical subproblems which are solved individually. Superimposing the subsolutions delivers the (generally non symmetric) field for the full problem. The symmetrical problems solved in this paper will clarify the advantage of MMP's symmetry exploitation concept.

It is one of MMP's strengths that the accuracy of a simulation may be reliably estimated within the numerical technique, i.e., for the validation of the results neither comparisons with other calculation techniques nor measurements are necessary. In spite of this fact, in specific cases a comparison with the results of a different technique may be quicker than the exclusive use of MMP's intrinsic validation tools.

A second point is that MMP — in particular its front ends, the PC version [2] and the unix version *mmptool*[1] [5] — offers very comfortable platforms for the graphical representation of both the errors and the results. This makes it possible to discuss both the physical behavior of the fields (by examining field plots) and the quality and reliability of the solution (by examining error plots).

[1] It must be stated that the two front ends are based on different philosophies. Therefore, they are really different and not only modified versions of the same program. All graphical representations in this paper are produced with the *mmptool*.

2 The Behavior of the Multipoles

Let us describe the behavior of multipole functions, first the well known point multipoles and then the line multipoles. The conventional multipole functions have a *local behavior* which means that they mainly 'act' close to their singularity although the functions are nonzero (but small) quite far away. We say that their area of (main) influence is a sphere, or more precisely, a spherical shell with a certain thickness. In the case of scattering at a sphere (see fig. 1) a point multipole forms an orthogonal set of expansion functions and the convergence is excellent. If the shape of the scatterer deviates from a sphere the convergence becomes poorer. The classical approach to avoid such type of problems is to use multiple multipoles, each of which is responsible for the field in a sphere around its singularity. The modeling process (the choice of the expansion functions) is essentially reduced to the geometrical problem of filling up a complicated scatterer with spheres. These spheres must be placed in such a way that the part of the boundary inside each sphere is simply shaped. The process has been completely automated and is part of the *mmptool* [5,6].

If the shape of a field domain includes sharp tips, edges, corners or thin wires, a large number of point multipoles is necessary. This means that the number of unknowns increases rapidly. However, the number is drastically reduced when line multipoles are used. The behavior of line multipole functions is essentially the same as that of point multipoles: Each function has large values close to the singularity and all functions of a line multipole together form a complete set for the expansion of any field in the environment of the singularity. The essential difference is the shape

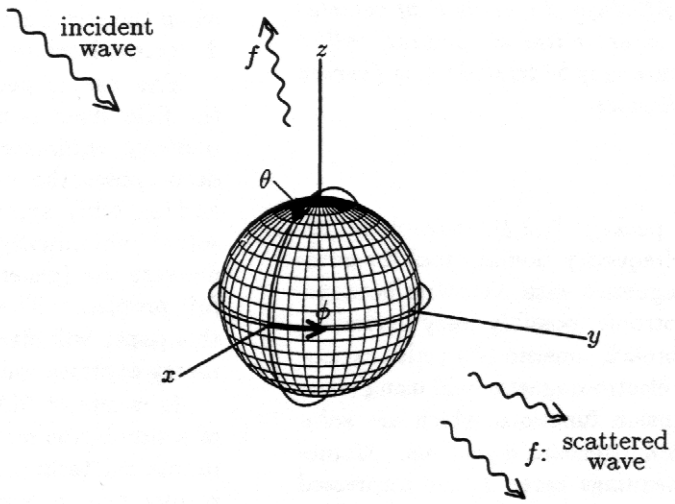

Figure 1: For any incident field, the scattered field f may be written as a sum of multipole functions, starting with a dipole and ending up with functions of higher order and degree. With the set of all multipoles up to the maximum order N, any variation of f along $\theta \in [0, \pi]$ describable by an N-th order polynomial in $\cos\theta$ may be represented exactly. Similarly, with the set of all multipoles up to the maximum degree M, any variation of f along $\phi \in [0, 2\pi]$ describable by an M-th degree Fourier series in ϕ may be represented exactly. Note that M and N may be chosen independently, but it is always true that $M \leq N$. For $N, M \to \infty$ the functions form a mathematically complete set of expansion functions.

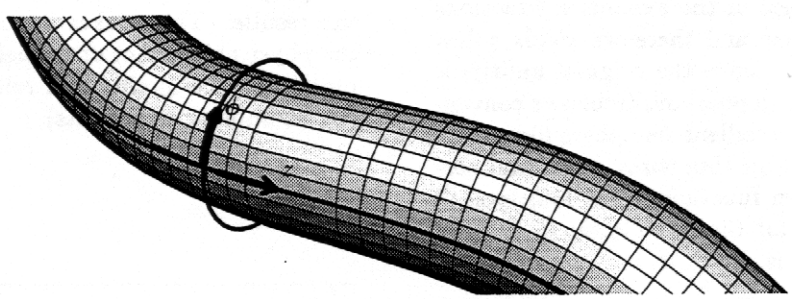

Figure 2: Curved line multipoles are singular on a line L of *finite* length, vary sinusoidally along ϕ and like a (Legendre-)polynomial along z (Fourier type longitudinal functions are also available). This behavior is strictly true only close to L since the coordinates z and ϕ are not unique away from the curved line L.

of the singularity: point multipoles are singular in a point, line multipoles are singular on a line (arbitrarily curved, with finite length, see fig. 2). Hence, the area of (main) influence of a line multipole is a sausage's surface (with thickness) rather than a sphere, and the modeling consists of filling the scatterer with sausages (line multipoles) *and*/or spheres (point multipoles). It is important to note that maximum order (behavior *along* the line) and maximum degree (behavior *around* the line) may be chosen independently from each other. This is very useful in practical applications. It is often known a piori that the field varies much more *around* an edge than *along* the edge. In fact this is the key point in the use of line multipoles versus point multipoles. Using line multipoles allows a drastic reduction of the number of unknowns in such cases.

3 The Use of the Multipoles

We shall describe the MMP modeling of three groups of problems. In the first group, we treat the scattering at spheres (conducting, dielectric, coated) as well as structures similar to spheres, in particular ellipsoids. This group is described mainly for reference and as an introduction, since such types of problems are not really problems for MMP. Both cpu times and storage requirements are extremely low, while the relative accuracy η is very high ($\eta < 10^{-4}$). In fact these are almost *analytical* solutions. The second group consists of three (well conducting) bodies illuminated by a plane wave. The bodies are a cone (with a tip and a curved edge), a cube (with edges and corners) and a 4-turn helical wire. The size of all the bodies in this group is roughly one wavelength λ. The third group consists of only one example: a ferrite tube on a long wire, where the excitation is not a plane wave but a current source at one end of the long wire.

3.1 Quantities to Be Discussed

In order to be able to compare different calculations of different problems, we define the following figures:

s_g: A three digit number defining the *geometrical* symmetry. The digits specify the reflective symmetries with respect to $x = 0$, $y = 0$ and $z = 0$ respectively. Each digit is either 0 (=no symmetry) or 1 (=symmetrical geometry). The examples below are self explanatory.

s_f: A three digit number defining the *decomposition of the field* into symmetrical and antisymmetrical parts. Each digit is either 0 (no decomposition), 1 (only the antisymmetrical part (odd part) must be computed), 2 (only the symmetrical part (even part) must be computed) or 3 (both the even part and the odd part must be computed) [2, 3:sect. 9.1]. Regardless of the situation, any field may be decomposed into symmetrical parts, but the decomposition is only useful when the geometry has the same symmetry. Therefore, a digit in s_f is only nonzero if the corresponding digit in s_g is nonzero. Certain fields need not be decomposed because they are already symmetrical, e.g., an x-polarized plane wave traveling in the z-direction has its own symmetry $s_f = 123$, and a complete decomposition yields only two nonzero parts. Note that any '3' in s_f doubles the number of subproblems to be solved.

N_{mat}: Number of matching points. Note that only one half (1 nonzero digit in s_g), one quarter (2 nonzero digits in s_g) or one eighth (if $s_g = 111$) of the full structure must be discretized, and N_{mat} covers only this fraction of the total structure.

N_{eq}: Number of equations. Each matching point is associated with up to six equations to match the different components of the electromagnetic field. Note that N_{eq} does not alter for different subproblems. All equations form a usually overdetermined system of equations.

N_{par}: Number of parameters (= number of expansion functions). For symmetrical problems $N_{par} = N_{par1} + N_{par2} + \ldots$, where $N_{par\,i}$ is the number of expansion functions in the i-th (anti-)symmetrical subproblem. Since the subproblems are computed one after each other, the memory requirement of the largest subproblem equals the memory requirement of the full problem. For large N_{par}, a subproblem with N_{par} parameters requires roughly $64 \times N_{par}^2$ bytes. Of course, N_{par} must be smaller than (or at the most equal to) N_{eq}.

t: Cpu time in seconds on a SPARC10 workstation. $t = t_1 + t_2 + \ldots + t_\eta$, where t_i is the cpu time for the i-th subproblem and t_η is the time for the calculation of the errors on all the matching points. Note that t_i includes both the calculation of the matrix elements and the least squares solution using Givens plane rotations.

η: The error, defined as the mean mismatching on all the matching points divided by the mean field values on the matching points. A special scaling is used, based on the field energy, in order to make electric and magnetic fields numerically comparable (see [2] or [3]).

3.2 Spheres and Sphere-like Structures

MMP's easiest example is the scattering at a sphere. We place the sphere's center at the coordinate origin and obtain $s_g = 111$. Since any orientation of the coordinate system yields the same s_g, the symmetry of the problem is equal to the symmetry of the incident plane wave: $s_f = 123$ (without any lack of generality.

See fig. 3.) and only two symmetrical subproblems must be solved. A single multipole expansion in the center of the sphere is necessary in order to end up with a practically exact solution ($\eta < 10^{-4}$). The tables below give the data for three cases, each at two different frequencies: $f_1 = 300\,\text{MHz}$ and $f_2 = 1\,\text{GHz}$. The three cases are the conducting sphere, the dielectric sphere ($\varepsilon_r = 4$) and the coated conducting sphere (thickness of dielectric coating: 1 cm, $\varepsilon_r = 4$). The diameter of the spheres is 1 m or — in terms of free space wave lengths — 1λ at $f = 300\,\text{MHz}$.

The expansion of the outer field (field in air) consists of a single point multipole expansion. In the second case (dielectric sphere) an additional regular expansion for the inner field is required, while in the third case (coated conducting sphere) both ingoing and outgoing waves have to be used to model the field in the coating. Note that it makes no sense to use line multipoles in this case, because the area of influence of a single point multipole covers the whole boundary.

The number of matching points is the same for each spherical surface. This explains why N_{mat} is doubled for the coated sphere. Beside this, it must be stated that three equations (boundary conditions) per matching point must be satisfied on a conductive surface (two for the tangential components of the total $\vec{E}$-field and one for the normal component of the total $\vec{H}$-field; these components should be zero), while six equations must be satisfied on the boundary between dielectric materials.

For the lower frequency ($f = f_1 = 300\,\text{MHz}$), the diameter of the sphere equals approximately the wavelength ($d \approx 1\lambda$), and we obtain:

case	η	$t_{1,2}$	t_η	$N_{\text{par1,2}}$	N_{mat}	N_{eq}
cond.	$7.4{\cdot}10^{-5}$	0.5	1	16	255	765
diel.	$9.2{\cdot}10^{-6}$	2	2	36	255	1530
coat.	$7.9{\cdot}10^{-6}$	6	5	54	510	2295

while for $f = f_1 = 1\,\text{GHz}$, it is $d \approx 3.3\lambda$:

case	η	$t_{1,2}$	t_η	$N_{\text{par1,2}}$	N_{mat}	N_{eq}
cond.	$2.6{\cdot}10^{-5}$	1.5	2	39	255	765
diel.	$1.5{\cdot}10^{-5}$	6	4	76	255	1530
coat.	$1.3{\cdot}10^{-5}$	18.5	11	115	510	2295

The same problem with an ellipsoid of revolution requires more computational effort. With respect to the coordinate system indicated in fig. 4, it is still $s_g = 111$, but if the angle of incidence is chosen arbitrarily, we must set $s_f = 333$. For simplicity's sake we choose a special polarization, defined as follows. First step: Choose the y-axis in such a way that the wave vector $\vec{k}_{\text{inc}}$ of the incident wave is parallel to the y-z-plane (no lack of generality). Second step: Use a special polarization, so that the electric vector of the incident wave ($\vec{E}_{\text{inc}}$) is parallel to the y-z-plane. This implies that the magnetic vector of the incident wave ($\vec{H}_{\text{inc}}$) points in $\pm x$-direction. In this case, $s_f = 233$ is sufficient and only four symmetrical subproblems must be solved.

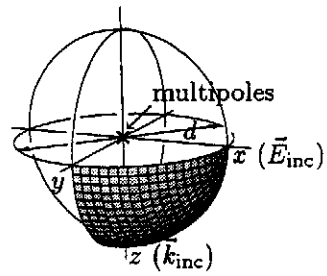

Figure 3: The x-polarized incident wave travels in direction z. Only one eighth of the sphere's surface must be discretized. ($d \approx \lambda$ or $d \approx 3.3\lambda$)

Using a single point multipole expansion in the center of the ellipsoid delivers relatively poor results, but if *two* multipole expansions are used (see fig. 4), the accuracy becomes much better. For comparison we give the figures for an ideally conducting ellipsoid with one and two multipole expansions as well as for a dielectric ellipsoid ($\varepsilon_r = 4$), all at $f = 300\,\text{MHz}$. For the field in the dielectric, a single regular expansion, i.e., an expansion with spherical bessel functions rather than spherical hankel functions and with its origin at the center is sufficient. Depending on the maximum order and/or degree of the multipoles, the number of parameters (N_{par}) varies slightly for the different symmetrical subproblems.

Again, only one eighth of the ellipsoid's surface must be discretized. We choose $N_{\text{mat}} = 348$ and obtain $N_{\text{eq}} = 1044$ for the conducting ellipsoid and $N_{\text{eq}} = 2088$ for the dielectric one. In this case, the following figures are obtained:

case	η	$t_{1,2}$	$t_{3,4}$	t_η	$N_{\text{par1,2}}$	$N_{\text{par3,4}}$
1 exp.	$3.0{\cdot}10^{-3}$	8	7	12	96	108
2 exp.	$4.7{\cdot}10^{-5}$	14	12	19	144	130
diel.	$2.3{\cdot}10^{-5}$	47	45	27	208	200

3.3 Structures with Edges, Tips and Wires

Whenever sharp edges or tips occur the field may become infinite at these locations. This is a problem for any numerical technique. MMP does not allow sharp edges but it does allow edges with rather fine roundings. The amount of calculation increases when the radius of curvature becomes smaller. Before the invention of the line multipoles [4], this was one of MMP's most severe limitations. Now, reasonably sharp edges may be modeled, but the amount of calculation still increases with the sharpness. Figure

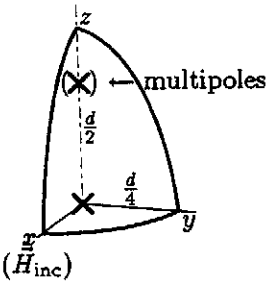

Figure 4: The larger diameter of the ellipsoid (a body of revolution with the z-axis as revolution axis) is roughly one wavelength ($d \approx \lambda$). The incident wave travels along an oblique straight line in the y-z-plane and $\vec{E}_{\text{inc}}$ is in the same plane, implying that $\vec{H}_{\text{inc}}$ is parallel to the x-axis.

5 gives both the geometrical models and the expansions for three different bodies (cone, cube and helix), all ideally conducting and with overall size $\approx \lambda$. Let us first discuss the symmetry and the expansions for these three examples. After that, we shall give the characteristic numbers for each problem and finally, we present some field plots and error plots and make some remarks.

For **the cone**, we have (with respect to the coordinate system in fig. 5) $s_g = 110$ and $s_f = 230$. This is related to an arbitrary angle of incidence, but a special polarization. Other than with the ellipsoid of revolution treated in the previous section, we choose $\vec{H}_{\text{inc}}$ parallel to the y-axis and both $\vec{E}_{\text{inc}}$ and $\vec{k}_{\text{inc}}$ parallel to the x-z-plane. Now this results in two symmetrical subproblems, since there is no geometrical symmetry with respect to $z = 0$. Therefore, a quarter of the cone's surface must be discretized. The density of the matching points is increased towards edges and tips. See the field plots below for the distribution of the matching points ($N_{\text{mat}} = 1837$, $\rightarrow N_{\text{eq}} = 5511$).

A single curved line multipole, placed in the center of curvature of the bottom edge, and four point multipoles, all placed on the z-axis, are used as expansions. It should be added that, in this particular case, a ringpole [7] could also be used. However, the application of ringpoles (for edges) is reduced to the case of circular edges while line multipoles are more general. We do not treat further applications of ringpoles in this paper.

The cube ($s_g = 111$, $s_f = 333$ [both arbitrary angle of incidence and polarization] $\rightarrow$ 8 symmetrical subproblems) needs three line multipoles for the edges and 5 point multipoles: one in the center, one on the diagonal $x = y = z$ and three on the coordinate planes $x = 0$, $y = 0$ and $z = 0$. It is important to note that point multipoles placed on the symmetry planes and oriented parallel to the symmetry plane with any of their local coordinate axes are preferred to those placed at an arbitrary location. This is due to the fact that a correctly placed and oriented point multipole expansion is inherently symmetry adapted, i.e., each single function is either even or odd with respect to a coordinate plane. MMP picks out only those needed, whenever the local coordinate system of the point multipole coincides with the global symmetry planes. The automatic pole positioner in the *mmptool* [5] takes care of this.

Only one eighth of the surface has to be discretized. We use 1727 matching points, leading to 5181 equations. Again, the matching point density is increased close to edges and corners (for details see the field plots below).

The last example in this group, **the helix**, has no reflective symmetries ($s_g = s_f = 000$). Thus, the full geometry must be discretized. It leads to 3472 matching points and 10416 boundary conditions. The expansion is quite simple: a line multipole along the wire for each turn and two point multipoles for the endcaps. Note that the point multipoles at the ends are essential: A line multipole does not form a complete set of expansion functions for this region. (However, as a matter of experience it is complete in the case of the cube's corner, where three orthogonal line multipole ends meet.) A single four turn line multipole rather than four one turn line multipoles would also be possible. We prefer four single turn line multipoles not only for reasons of higher flexibility and the (quasi) periodicity of the field, but also because only one turn of the helical line must be specified. (NB: The line associated to a curved line multipole is specified in local coordinates of the expansion and is stored in a file named `mmp_lyy.xxx` [4] which may be produced with the *mmptool* [5].)

Looking at cpu times and mean errors for these three examples, we find that the accuracy is lower than in the previous cases, but still good for practical purposes (below 4%). On the other hand, cpu times are higher. The following values were obtained (we give mean values for the symmetrical subproblems, since the deviation among the subproblems is only small):

case	η	t_i	t_η	$N_{\text{par}\,i}$	N_{mat}
cone	$1.2{\cdot}10^{-2}$	2131	1371	691	1837
cube	$3.8{\cdot}10^{-2}$	1979	10499	468	1727
helix	$1.7{\cdot}10^{-2}$	9194	1900	1152	3472

Note that the number of unknowns for the complete problem with symmetrical bodies is higher: There are $2 \times 691 = 1382$ unknowns for the (slightly symmetrical) complete field of the cone and $8 \times 468 = 5148$ unknowns for the completely arbitrary field around the cube. Both numbers are significantly higher[2] than for the helix. Thus, we see that —

[2] A nonsymmetrical field around the cone yields $4 \times 691 = 2764$ unknowns.

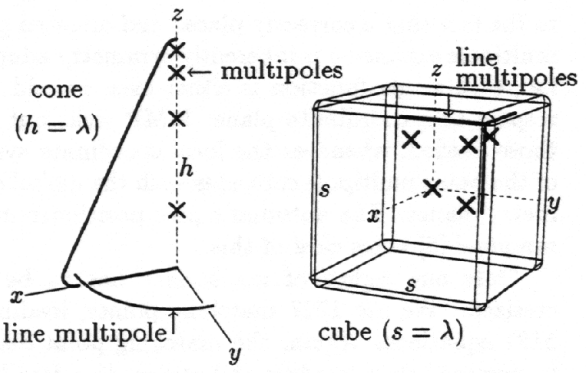

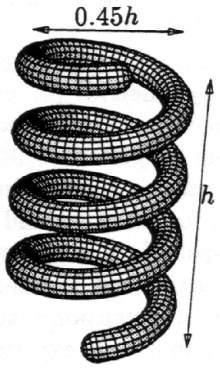

4-turn-helix $(h = \lambda)$

Figure 5: Three different 1λ-sized bodies, a cone of revolution, a cube and a helical wire. In all three cases line multipoles are useful for field modeling. The center of each rectangle on the helix' surface is one matching point. See figs. 6, 8 and 11 for the distribution of the matching points on the surfaces of the cone and the cube respectively.

at a given accuracy — the number of unknowns increases with the deviation from the 'expansion's optimal shape' (sphere for point multipoles, sausage for line multipoles).

The very first quality test for a calculation is the distribution of the errors (local mismatching) on the boundaries. Figure 6 shows the error distribution on that part of the cube which is really discretized (the eighth in the first octant of the coordinate system). For clarity the whole cube has been drawn. Note that due to the nonsymmetrical field the error has different values on the rest of the cube. Nevertheless the distribution on the first octant gives a good impression. The absolute amount of the error values must be compared with the incident field or — e.g. at tips — with the total field close to the boundary. In this particular example we notice that the maximum error occurs neither at the edge nor at the corner but on the flat surface. This indicates that the line multipoles used for the modeling of the edge and corner field are a better choice than the point multipoles for the flat surface field. This could be changed by using higher order point multipoles or — as an alternative — more point multipoles. Figure 8 shows the error

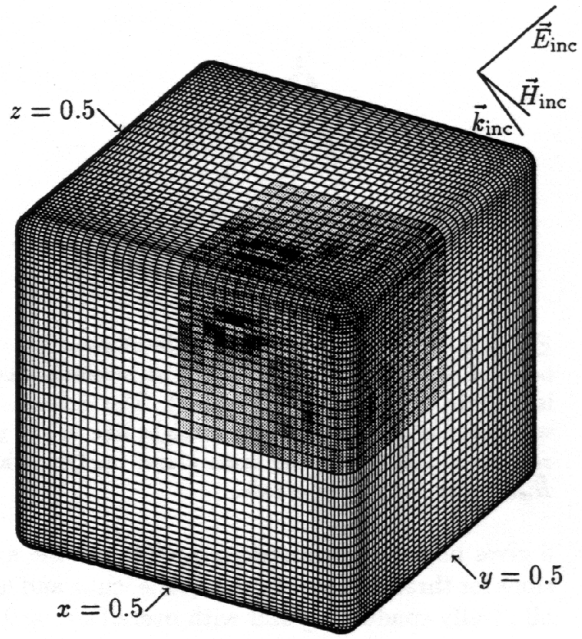

Figure 6: The full cube model. Note that only the front eighth (shaded proportional to the local error) must be discretized, and all calculations are done on this eighth only. At the top right the orientation of the incident plane wave is shown. Note that in this particular example, $\vec{H}_{\text{inc}}$ is parallel to the cube's top $(z = 0.5)$ and $\vec{k}_{\text{inc}}$ is parallel to $(-1, 0.527, -2)$.

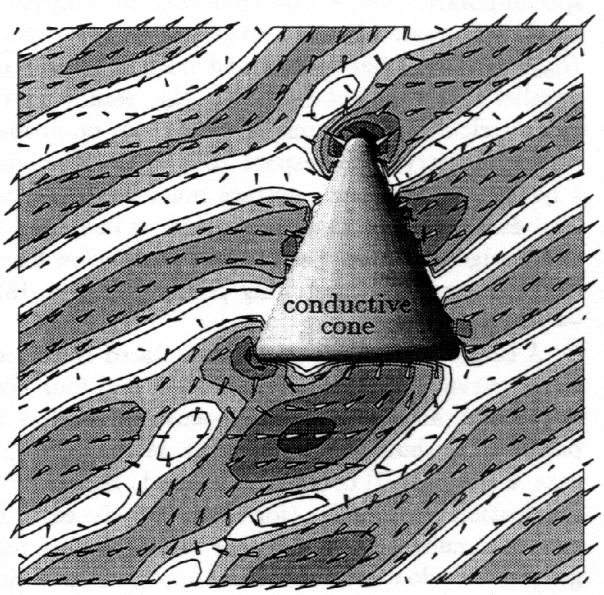

Figure 7: The picture shows the instantaneous value of the total electric field $\vec{E}$ in the symmetry plane $y = 0$. The triangles point in the direction of $\vec{E}$ and the contour lines indicate its magnitude. The incident wave travels from bottom right to top left. The animated representation of this field with the *mmptool* shows the creeping of the wave around the bottom left edge of the cone. See also fig. 10 for $\langle \vec{S} \rangle$.

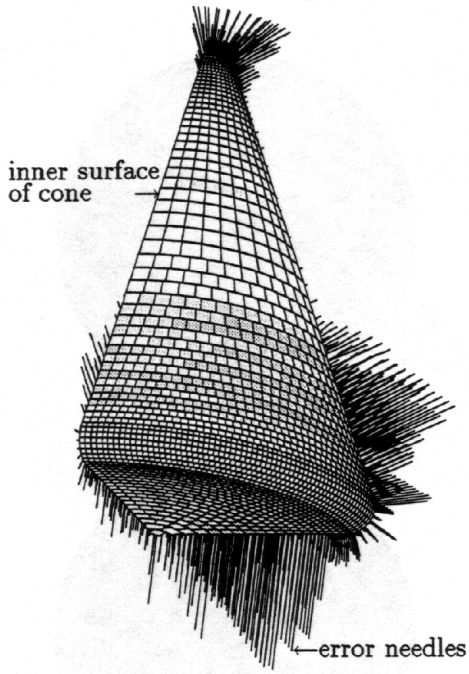

Figure 8: The error distribution on one quarter of the cone. The visible inner surface is shaded proportional to the local absolute error η_{loc}. On the outer surface (not visible), surface orthogonal needles (partly visible) are attached with length proportional to η_{loc}. This is called 'hedgehog' representation of the error. The largest errors occur somewhat away from the bottom edge. These errors could be reduced with one or two additional line multipoles placed close to the maximum η_{loc}. Note the higher matching point density close to both the edge and the tip. For the tip see also fig. 11.

distribution on the cone. Again the maximum error occurs on the flat bottom surface. This is obvious since the area of influence of the multipoles, i.e., a spherical surface of a certain thickness for point multipoles, can hardly follow a flat surface.

A second quality test is a closer look at the behavior of the field in the space around the scatterer. Figures 7 and 9–11 show the behavior of the total electromagnetic field close to the different scatterers (nearfield representations). These pictures verify the quality of the solutions. It is good practice to first inspect the power flux (Poynting vector $\vec{S}$). This vector (in particular also its time mean value $\langle\vec{S}\rangle$) must be tangential to the scatterer's surface. Any component normal to the surface is erroneous and indicates a local insufficiency of the expansion. On the other hand one can learn what really happens around the scatterer. As a matter of experience the energy often takes unexpected ways although its behavior may be clearly explained a posteriori. One of the most obvious effects is the 'creeping' around corners and along curved surfaces (see figs. 7 and 9). This effect is only

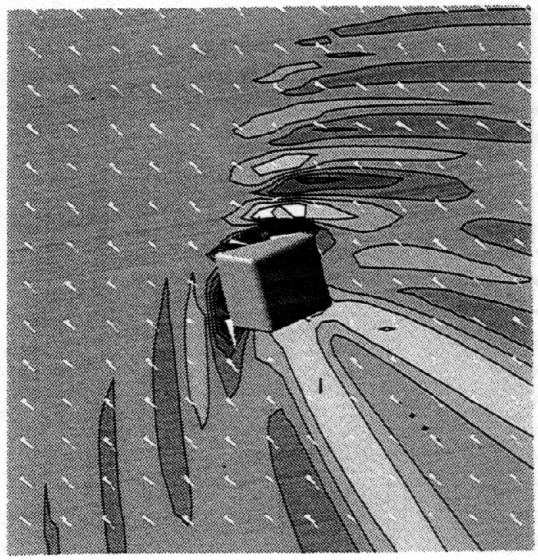

Figure 9: This picture shows the total power flux (Poynting vector, time mean value) around the cube in the $\vec{E}$-plane of the incident wave. The center of the oblique field representation square coincides with the cube's center and is oriented so that the incident wave is traveling in the diagonal form top left to bottom right and $\vec{E}_{\text{inc}}$ is parallel to the top right – bottom left diagonal. Note the interference of the incident wave with the scattered wave reflected by the cube's plane sides, the creeping around the edges and the double-branched shadow. The white triangles indicate the direction and the underlying contour lines show the absolute value.

present if the electric field is large (only the normal component, of course!). The instantaneous value of the electric and magnetic field, respectively, are also instructive although their behavior is more complicated. Animated representations give deepest insight into the physical process. Both the *mmptool* [5] and also the PC-based front end [2] have powerful movie capabilities. The PC-version's movie feature is even more sophisticated.

In many practical applications, only the scattered farfield is requested. Figure 12 represents the farfield (radiation pattern) of both cone and helix. This type of output is produced in the very same way as near field plots: One just specifies a surface in the farfield zone and computes the (scattered) field on it.

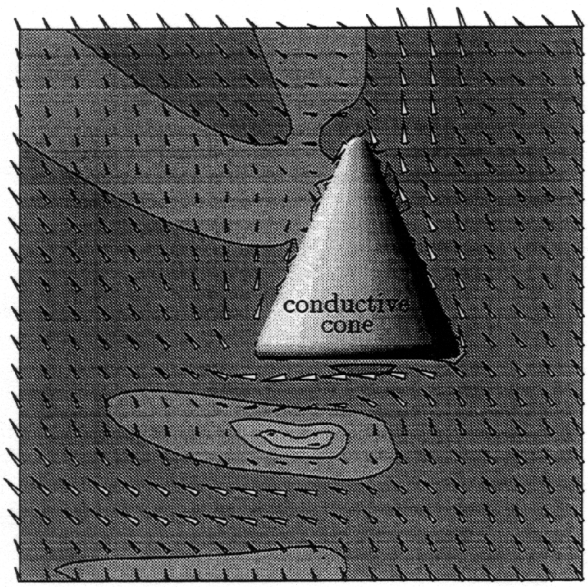

Figure 10: The time mean value $\langle \vec{S} \rangle$ of the total Poynting field $\vec{S}$, drawn on the same rectangle as in fig. 7. The interference of the incident wave with the scattered wave reflected by the underside of the cone produces the light 'field free' zone. The 'shadow' at the top left is separated in two branches which is typical for 1λ-sized scatterers. See also fig. 9.

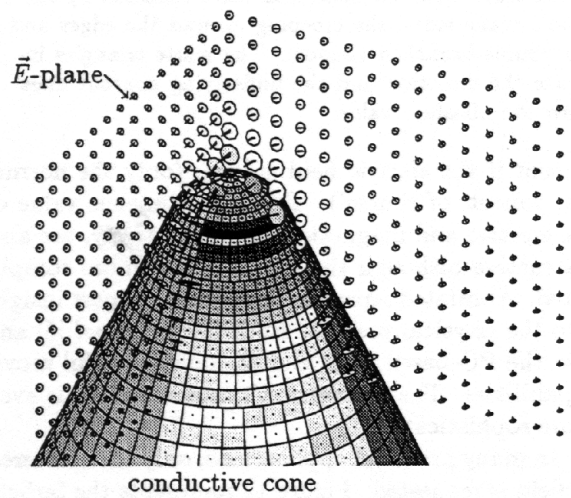

Figure 11: This picture shows the behavior of the total Poynting vector's time mean value ($\langle \vec{S} \rangle$) close to the cone's tip. Note the diffraction ('creeping' around the tip) at the top left in the $\vec{E}$-plane. The incident wave comes from bottom back (wave vector $\vec{k}_{\text{inc}}$ parallel to $\vec{E}$-plane).
The representation of the field with 'thumbtacks' (pointing in the direction of $\langle \vec{S} \rangle$) gives a good impression of the three-dimensionality of the field.
The matching points in the first quarter (both $x > 0$ and $y > 0$) are gray scaled proportional to the local error of the solution: Darker rectangles denote larger absolute errors. Visible maximum: $27\frac{\text{mV}}{\text{m}}$ with an amplitude of the incident wave of $1\frac{\text{V}}{\text{m}}$.

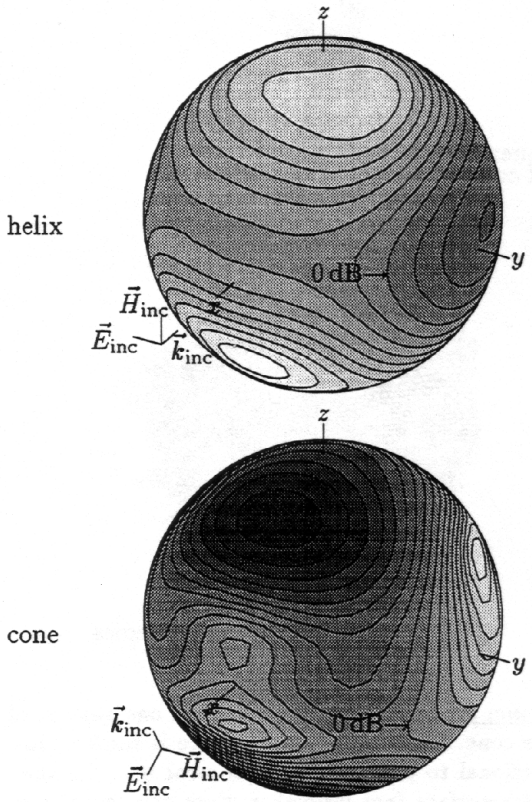

Figure 12: Radiation patterns for helix (above) and cone (below). The contour lines are drawn on a spherical surface (radius of sphere = 10λ) and show the radial component of the Poynting-vector's time mean value of the scattered field only. The amplitude of the incident wave is the same for both cases and the gray scales are also equal. Darker area's denote higher values.
Note the different orientations of the incident wave in both cases ($\vec{E}_{\text{inc}}$, $\vec{H}_{\text{inc}}$ and $\vec{k}_{\text{inc}}$ form a right hand system). The cone as a more solid body has a higher scattered field.

3.4 A Ferrite Tube on a Wire

Our last example is a problem from electromagnetic compatibility (EMC). We study the influence of a ferrite tube placed on a long straight cable. (The tube is mounted in order to attenuate waves propagating along the wire, and this particular shape of the tube is used in the so-called conductive testing.) The geometric model has symmetry of revolution (see fig. 13). A full symmetry decomposition of an arbitrary field would involve an infinite number of subproblems. MMP does not support this type of symmetry, but the symmetry could be partially exploited by two reflective symmetries. We prefer a different procedure and perform the symmetry exploitation 'by hand'. Since our excitation (current source at right end in fig. 13, top) has the same symmetry as the geometry, we know that the scattered field must also have symmetry of revolution. Thus,

it is sufficient to use only expansion functions with this symmetry and consequently, not only the geometry may be fully described in a half plane, but also the field matching need only be performed on *lines* (the contour in fig. 13, bottom) rather than on the full surfaces.

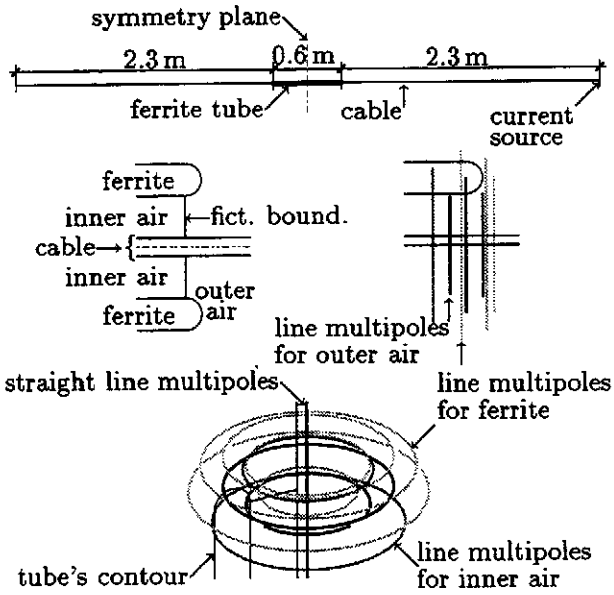

Figure 13: Top: A long straight wire with an impressed current at the right end and zero current at the left end. The ferrite tube in the center is mounted in order to reduce wave propagating along the wire.
Middle left: Zoom of the ferrite tube's right front. The fictitious boundary allows different expansions for inner and outer air.
Middle right: Circular line multipoles with constant intensity along the whole circle produce a field with circular symmetry and relative strong variation close to the circles.
Bottom: The same as middle right, but in a perspective view. The straight line multipoles on the cable axis are for inner air, outer air and ferrite. Inner and outer air line multipoles overlap close to the fictitious boundary.
Further data: diameter of the infinitely well conducting cable: 4 mm; inner and outer radii of ferrite tube: 11.2 mm and 18.3 mm; relative permeability of ferrite: $\mu_r = 160 + 37i$ at $f = 30$ MHz and $\mu_r = 29 + 110i$ at $f = 100$ MHz; relative permittivity of ferrite: $\epsilon_r = 15$.

Using a cylindrical r-ϕ-z coordinate system with z-axis along the cable, we find that only three components of the electromagnetic field (E_r, E_z and H_ϕ) are nonzero, while $E_\phi = 0$ and $H_r = H_z = 0$. This implies that only E_z must be matched on the cable's surface, while on the fictitious air–air boundary as well as on the air–ferrite boundary, three boundary conditions are necessary.

With respect to the symmetry plane $z = 0$ (see fig. 13, top), a normal MMP symmetry is used. Due to the fact that there is only one current source at the right end, we have $s_g = 001$ and $s_f = 003$ resulting in two symmetrical subproblems. The solutions for two frequencies yield the following characteristic figures:

f[MHz]	η	$t_{1,2}$	t_η	$N_{\text{par1,2}}$	N_{mat}
30	$2.7{\cdot}10^{-3}$	643	1194	256	984
100	$3.8{\cdot}10^{-2}$	670	1254	256	984

Note that both N_{mat} and N_{par} are relatively small. This is due to the field's symmetry of revolution. The result for $f = 100$ MHz seems to be quite accurate for practical purposes. However, a closer look at the distribution of the local errors and in particular at the field shows that the solution is not very good (see fig. 16). This example shows that a small mean error is not always sufficient for a good solution.

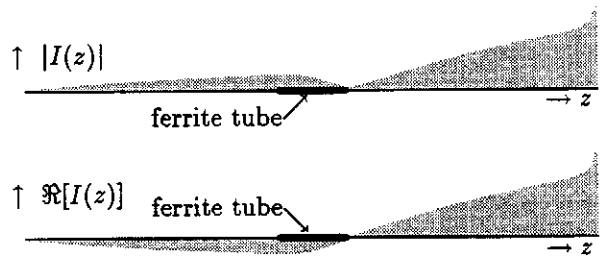

Figure 14: The current distribution on the wire with ferrite tube at $f = 30$ MHz. Note that the wire is roughly half a wave length long and the source is placed at the right end.

4 Summary

It has been shown that MMP delivers almost exact solutions (mean error $\eta < 0.01\%$) for conducting, dielectric and coated sphere like structures. Also the field of more complicated bodies may be calculated very accurately ($\eta < 4\%$). The amount of calculation increases when sharp edges or tips are present, and at the same time, the accuracy decreases. Through the use of (curved) line multipoles, the modeling process (choice of expansion functions) is simplified and the range of MMP applications is significantly enlarged towards more practical situations. The notion of the area of influence for multipoles (spherical shell for point multipole, sausage shaped shell for line multipole) is helpful. The error distributions show that the mismatching is low as long as the boundaries follow the areas of influence of the multipoles.

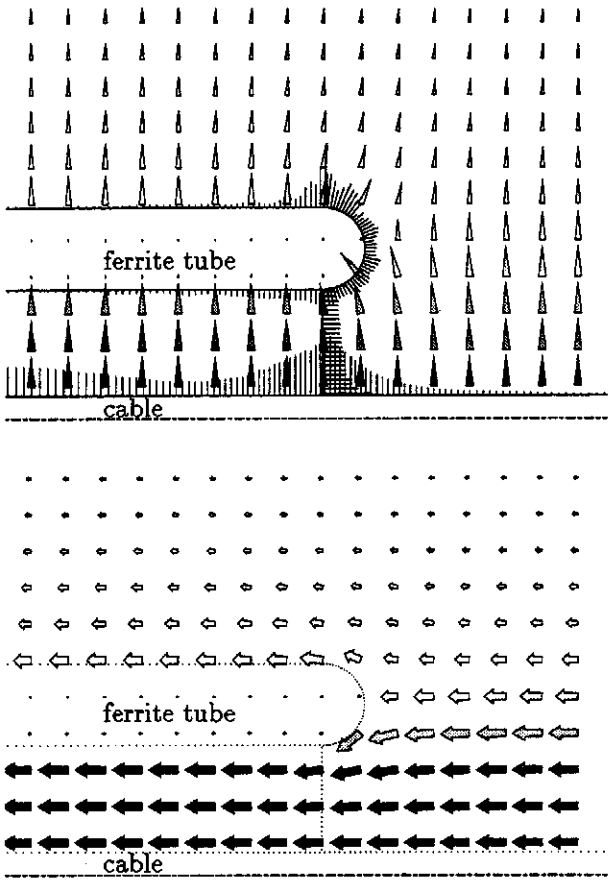

Figure 15: The field at the front end of the ferrite tube at $f = 30\,\mathrm{MHz}$. Top: electric field and hedgehog error representation. The maximum error occurs on the cable's surface, close to the fictitious boundary between inner air and outer air and represents in this case the longitudinal component of the electric field (actual value in ratio to the normal component: 0.4%). Note that the matching point density is increased towards the front. Bottom: Time mean value of Poynting field. Note that according to the principle of least action the energy hardly penetrates the ferrite.

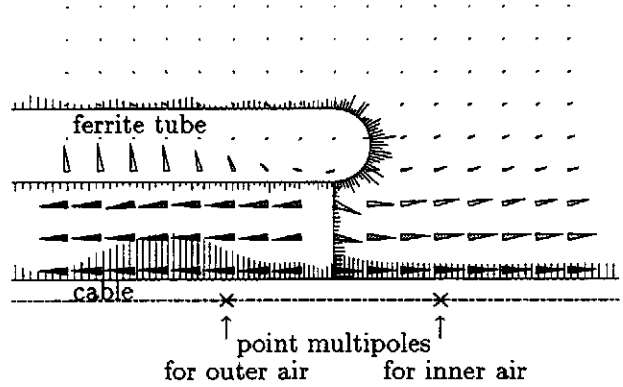

Figure 16: The (obviously erroneous!) Poynting field (time mean value) at the front end of the ferrite tube at $f = 100\,\mathrm{MHz}$. Although the relative errors on the cable's surface are small, the solution is not as good as one might believe. The divergence of the Poynting field at the fictitious boundary indicates a numerically small but physically large error. Errors of this type may occur when the absolute values of the field vary strongly at different parts of the full structure. They may be corrected with individual weighting of the boundary conditions.

5 References

[1] Ch. Hafner, *The Generalized Multipole Technique for Computational Electromagnetics*, Artech House Books, 1990.

[2] Ch. Hafner and L. Bomholt, *The 3D Electrodynamic Wave Simulator*, J. Wiley, 1993.

[3] P. Leuchtmann, *The Generalized Multipole Technique (GMT) and the Multiple Multipole Program (MMP): Theory and Practical Use in Computational Electromagnetics*, 110 pages, 1993 (a basic introduction, available from the author).

[4] P. Leuchtmann and M. Gnos, "Curved Line Multipoles for the MMP-code," in *10th Annual Review of Progress in Applied Computational Electromagnetics (ACES), Conference Proceedings*, (Monterey), Mar. 1994.

[5] P. Regli, *mmptool*, public domain program, available through ftp anonymous on sirius.ethz.ch (129.132.41.1), directory mmp, ETH Zürich, Nov. 1993.

[6] P. Regli, *Automatische Wahl der sphärischen Entwicklungsfunktionen für die 3D-MMP Methode*, Diss. ETH Nr. 9946, Zürich, 1992.

[7] J. Zheng, "A new expansion function of GMT: the ringpole," in *7th Annual Review of Progress in Applied Computational Electromagnetics (ACES), Conference Proceedings*, (Monterey), pp. 170–173, Mar. 1991.